

Note: This is a draft of a paper submitted for publication. Contents of this paper should not be quoted or referred to without permission of the author(s).

To be presented at the International Memorial Symposium Devoted to the
70th Anniversary of Prof. M. O. Krivoglaz,
“New Diagnostic Techniques Based on the Synchrotron Radiation Beams”
Alushta, the Crimea, Ukraine, September 6-12, 1999
and to be published in the journal *Metal Physics and Advanced Technologies*

**Microbeam X-Ray Diffuse Scattering Study of
Ion-Implanted Induced Defects in Silicon**

B. C. Larson, M. Yoon, J. Z. Tischler, G. E. Ice, and T. E. Haynes
Solid State Division, Oak Ridge National Laboratory
P.O. Box 2008, Oak Ridge, Tennessee 37831-6030

P. Zschack
UNI-CAT Beam Line, Advanced Photon Source,
Argonne National Laboratory
Argonne, IL 60439

"The submitted manuscript has been authored by a contractor of the U.S. Government under contract No. DE-AC05-96OR22464. Accordingly, the U.S. Government retains a nonexclusive, royalty-free license to publish or reproduce the published form of this contribution, or allow others to do so, for U.S. Government purposes."

prepared by
SOLID STATE DIVISION
OAK RIDGE NATIONAL LABORATORY
Managed by
LOCKHEED MARTIN ENERGY RESEARCH CORP.
under
Contract No. DE-AC05-96OR22464
with the
U.S. DEPARTMENT OF ENERGY
Oak Ridge, Tennessee

August 1999

Microbeam X-Ray Diffuse Scattering Study of Ion-Implantation Induced Defects in Silicon

B. C. Larson, M. Yoon, J. Z. Tischler, G. E. Ice, and T. E. Haynes
Oak Ridge National Laboratory, Oak Ridge, TN 37830

And

P. Zschack

UNI-CAT Beam Line, Advanced Photon Source, Argonne National Laboratory,
Argonne, IL 60439

Abstract

Submicron resolution x-ray beams have been used for diffuse scattering investigations of the size, concentration, type, and depth dependence of ion-irradiation induced defects in silicon irradiated with 10-MeV Si ions at 300°C. Diffuse scattering measurements in the asymptotic (Stokes-Wilson) diffuse scattering region near Bragg reflections have been carried out in cross-section, as a function of implant depth, using x-ray microbeams focused to 0.7 μm by Fresnel zone plate optics. Cross-section microbeam measurements are analyzed in terms of the size distributions for vacancy and interstitial loops as a function of depth, and the cross-section diffuse scattering technique is compared to alternative measurements for studying ion-implantation induced defects.

I. Introduction

The analysis of diffuse scattering near Bragg reflections represents a powerful method for the study of defect clusters that induce lattice distortions in crystalline materials. Krivoglaz[1], Trinkaus[2], and Dederichs[3] systematically analyzed the form and intensity of the Huang diffuse scattering resulting from the long-range elastic distortion fields surrounding point defects and defect clusters. Their work further considered the scattering in the so-called asymptotic or Stokes-Wilson region, beyond the Huang scattering region, that can be characterized in terms of local Bragg scattering from the relatively large distortions near defect clusters[4]. In general, the asymptotic diffuse scattering associated with the large lattice displacements near clusters cannot be specified analytically. However, numerical diffuse scattering cross-sections for this region can be obtained with the use of numerically calculated elastic displacement fields for loops and precipitates[5,6].

The availability of reliable diffuse scattering cross-sections for defect clusters has made it possible to use diffuse scattering as a tool to investigate irradiation induced defects in crystals. X-ray diffuse scattering has been used in a large number of studies of electron, neutron, and ion-irradiated metals, semiconductors and insulators. Electron and neutron irradiations produce defects distributed uniformly throughout bulk samples; however, ion-irradiations typically involve penetrations of only a few microns near surfaces and result in defect distributions that are strongly depth dependent. Understanding defect interactions as well as the generation and annealing characteristics

of ion-irradiation induced defects has become increasingly important as ion-implantations are incorporated into electronic device manufacture and as length scales decrease.

In this paper we discuss the use of submicron spatial resolution x-ray microbeams for depth dependent studies of ion-implantation induced defects in silicon. The results of depth dependent differential diffuse scattering measurements, made in cross-section on self-ion irradiated silicon, are presented in terms of size distributions and point defect concentrations for vacancy and interstitial loops, and relative merits of cross-section and plan-view diffuse scattering techniques are discussed.

II. Theory

The scattering cross-section for diffuse scattering from randomly distributed defects is given for kinematical scattering conditions by [7]

$$\frac{d\sigma(\mathbf{K})}{d\Omega} = |r_e f(\mathbf{K})|^2 |A(\mathbf{K})|^2, \quad (1)$$

where r_e is the classical electron radius, $f(\mathbf{K})$ is the atomic scattering factor, \mathbf{K} is the scattering vector given by $\mathbf{K} = \mathbf{H} + \mathbf{q}$. \mathbf{H} is a reciprocal lattice vector and \mathbf{q} is a vector in the Brillouin zone. $A(\mathbf{K})$ is the diffuse scattering amplitude for randomly distributed defects, which in the single defect approximation is given by

$$A(\mathbf{K}) = \sum_i e^{i\mathbf{K}\cdot\mathbf{r}_i^d} + \sum_j e^{i\mathbf{q}\cdot\mathbf{r}_j} \left(e^{i\mathbf{K}\cdot\mathbf{s}_j} - 1 \right), \quad (2)$$

where the first term represents the direct Laue scattering from the atoms in the defect cluster (i. e. loop, precipitate, loose aggregate) and the second term represents the scattering from the surrounding atoms that are displaced \mathbf{s}_j from their regular lattice positions by the distortion field surrounding the defect clusters. Techniques for numerical evaluation of Eq. (2) have been presented in detail elsewhere [7,8,9] and are not discussed here.

Experimentally measured diffuse scattering is related to the scattering cross-sections for defect clusters through [10]

$$I(\mathbf{K}) = \frac{I_o}{2\mu_o} \sum_i c_i(R_i) \frac{d\sigma_i(\mathbf{K}, R_i)}{d\Omega}(\Delta\Omega), \quad (3)$$

where I_o is the incident beam power, μ_o is the linear absorption coefficient, $c_i(R_i)$ is the volume concentration of defect clusters of radius R_i , and $\Delta\Omega$ is the solid angle subtended by the detector.

For the investigation of the size and type of loops or clusters in a defect distribution, it is convenient to use the asymptotic or Stokes-Wilson diffuse scattering region ($q > 1/R$),

for which the intensity goes as $\sim (bR)/q^4$. This is in contrast with the Huang region scattering ($q \ll 1/R$) for which the intensity falls off as $\sim (bR^2)/q^2$, where R is the defect radius. For the case of loops, the local Bragg scattering interpretation [4] of scattering from the asymptotic region carries information on the vacancy/interstitial nature through sensitivity to the sign of the strain in the immediate vicinity of the loops, as depicted in Fig.1. The lattice models in the figure show schematically the distorted regions surrounding a precipitate and a loop. The precipitate model illustrates specifically that the lattice contraction associated with an undersized coherent second phase particle expands (i.e. stretches) the lattice immediately surrounding the particle. The interstitial loop model emphasizes that interstitial loops have predominantly compressed regions near the loop plane. Of course, vacancy loops generate a locally expanded region near the loop plane as surrounding lattice planes relax into the vacant loop area.

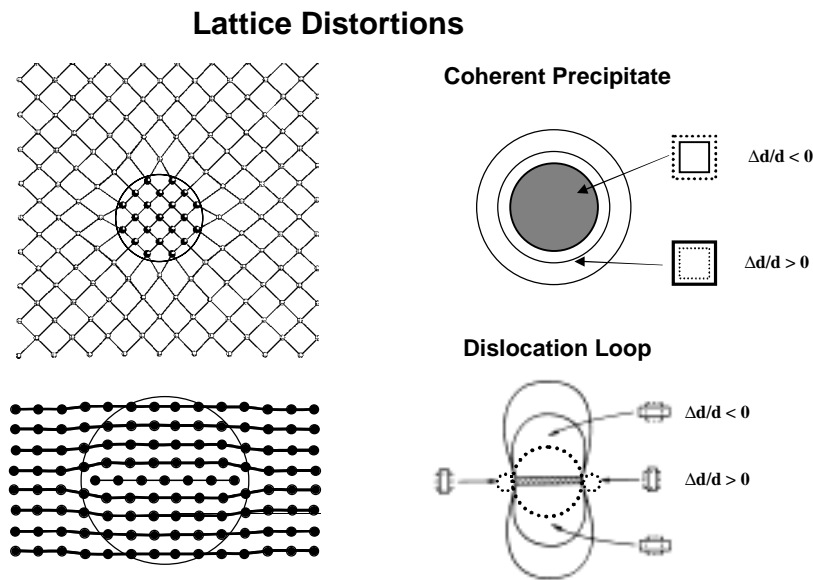


Fig. 1. Schematic views of the lattice distortions around an undersized coherent precipitate and an interstitial loop. The precipitate has a lattice parameter smaller than the host and gives rise to distortions expanding the surrounding lattice. The dislocation loop has lattice compression both at the loop plane and in the surrounding host lattice. The large dashed circles indicate regions of nearly constant lattice parameter.

Numerical calculations of lattice distortions around loops have shown the strain in regions immediately above (and below) the plane of edge type loops to be given by $\Delta d/d \approx -b/4R$ for metals[5, 10], where b is the Burgers vector of the loop. Therefore, for loops oriented normal to H , there is a strong local enhancement in the $\sim q^{-4}$ fall-off of the asymptotic scattering in the region $q = bH/4R$. Models for infinitesimal size defects have r^{-2} displacement fields for all r , which gives rise to an extended q^{-4} intensity region. On the other hand, the displacements for dislocation loops reach a limiting value of $b/2$ as r goes to zero, and therefore do not have continuously diverging r^{-2} displacement fields. In fact, the displacements become nearly linear in r over a spherical region with the radius of the loop. This leads to a nearly constant lattice parameter as mentioned above, so the diffuse scattering is enhanced near $q = bH/4R$ and falls off much more rapidly than q^{-4} for

larger q -values. It is important that the relationship for the position of the enhanced intensity contains both b and R , because the sign of b (i.e. vacancy or interstitial type) can be determined by the direction of q relative to H , and the radius R can be inferred from the magnitude of q . It is further important to recognize that there are no regions of significant size with expanded lattice parameters for interstitial loops, implying that there will be no significant amount of scattering for negative q associated with interstitial loops [10].

For coherent precipitates, the r^{-2} form of the distortion field is cut off by the finite size of the precipitate, below which the displacements fall linearly to zero rather than continue to rise as r^{-2} . The coherent particle represents a region with a constant lattice parameter, which results in a relatively strong local Bragg reflection. In contrast to the case for loops, however, the direct Laue scattering from the precipitate lies on the opposite side of the host crystal Bragg peak from that of the distorted host diffuse scattering. These effects have been appreciated in general for some time [11, 12, 13], and they have been discussed quantitatively in connection with numerical diffuse scattering calculations for precipitates by Iida and Larson [6]. The q^{-4} region is truncated by the finite size of the precipitate, but the strong enhancement analogous to the case of loops is at $q = -\epsilon H$, where ϵ is the fractional change in the lattice parameter of the precipitate relative to the host.

III. Experiment

In this investigation, $\langle 001 \rangle$ oriented floating zone silicon crystals were irradiated with 9×10^{16} 10 MeV Si ions at a temperature of 300°C. The crystals were subsequently cleaved along $\{110\}$ planes normal to the implanted surface and Syton polished to allow cross-section diffuse scattering measurements as a function of depth along the implantation direction [14]. Monochromatic x-ray microbeams with an energy of 8.95 KeV were generated on the UNI-CAT beam line at the Advanced Photon Source using a 150 μm diameter compound Fresnel zone plate with a 5.6 cm focal length [15]. As illustrated schematically in Fig. 2, a 20 μm order-sorting aperture was used to eliminate higher order zone-plate contributions from the focused beam, and a 25 μm tungsten wire was inserted in the incident beam to eliminate any unfocused radiation from passing through the order-sorting aperture. Fig. 2 shows the scattering geometry in which a 0.7 μm (source size limited) focused x-ray beam was used for diffuse scattering measurements.

Diffuse scattering measurements were performed radially in q along the $[220]$ reciprocal lattice direction near the (220) Si reflection; slit collimation was employed in the diffracted beam and a scintillation x-ray detector was used. The depth dependent measurements were carried out in cross-section by translating the Si sample along the $[001]$ implantation direction using an inchworm based translation stage encoded to 50 nm. Scattering measurements were performed $>10 \mu\text{m}$ into the crystal to determine the diffuse scattering background for a defect free crystal.

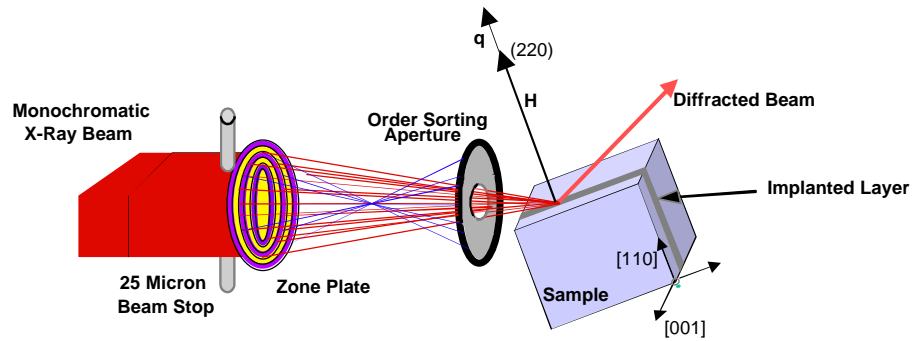


Fig. 2. Microbeam diffuse scattering geometry showing the Fresnel zone plate focusing element, a wire central beam stop, an aperture to limit higher order focused x-rays, and the implanted sample orientation and scattering geometry.

IV. Results

Figure 3 shows a crystal translation scan monitoring the total diffuse scattering as a function of depth along the [001] direction for a silicon crystal implanted along the [001] direction. The diffuse scattering in the figure was measured at $q = 0.04 \text{ \AA}^{-1}$ in the [220] direction, radially outward from the (220) reciprocal lattice point. The sharp step in the intensity defines the (depth $d = 0$) surface position for the crystal, and the intensity above the dashed line represents the diffuse scattering from the implantation induced defects. We note a very weak plateau of diffuse scattering in the first 2-3 microns below the surface followed by a large peak in the diffuse scattering centered at a depth of $4.25 \mu\text{m}$, which corresponds to the range of the implanted silicon ions. Since the ions are confined to depths of $< 5 \mu\text{m}$, the intensity deep in the crystal provides a measure of the background diffuse scattering (thermal, Compton, Bragg tails). The logarithmic scale of the plot in Fig. 3 indicates that the diffuse intensity in the plateau is only a few percent of the intensity at the peak. We note from the rounded corner of the step at $d = 0$ that the $\sim 0.7 \mu\text{m}$ resolution of the x-ray beam limits the measurement of very small intensities above background to depths greater than a micron below the surface.

Electron microscopy measurements made on this sample [16] and on silicon implanted under similar (high temperature, high fluence) conditions have shown the presence of a region with few visible defects in the first few microns below the surface. This region of $> 4 \mu\text{m}$ was followed by an extremely dense band ($\sim 0.3\text{-}0.4 \mu\text{m}$) of defect clusters in the range of the implanted ions.

It is of course understood that the implanted ions constitute excess interstitial atoms that do not have corresponding vacancies with which to annihilate. In addition, the forward momentum of the interstitials (as they are created by the impinging implanted ions) leads to a local imbalance in the number of vacancies and interstitials in favor of vacancies near the surface. This process leads to an additional oversupply of interstitials near the damage peak and the end of range. The magnitude of these effects is a

function of the local defect concentration gradients as well as the extent of thermal and radiation induced annealing/annihilation of defects. Because vacancy rich regions give rise to enhanced diffusion, these issues are highly important for device manufacturing considerations, unfortunately, they have been difficult to study quantitatively because of the difficulty of identifying the presence of vacancy clusters by electron microscopy. Spatially resolved x-ray scattering is employed here to identify the nature as well as the concentration and size distributions of the defect clusters as a function of depth. The diffuse scattering analyses will be made in terms of vacancy and interstitial loops, considering the preponderance of interstitial dislocation loop type defects observed by TEM in neutron and ion irradiated silicon. Only relative concentrations of loops will be presented here because an absolute measure of the incident focused was not made during these measurements. Future work will address absolute concentrations and the assumption of loop type defects will be discussed later..

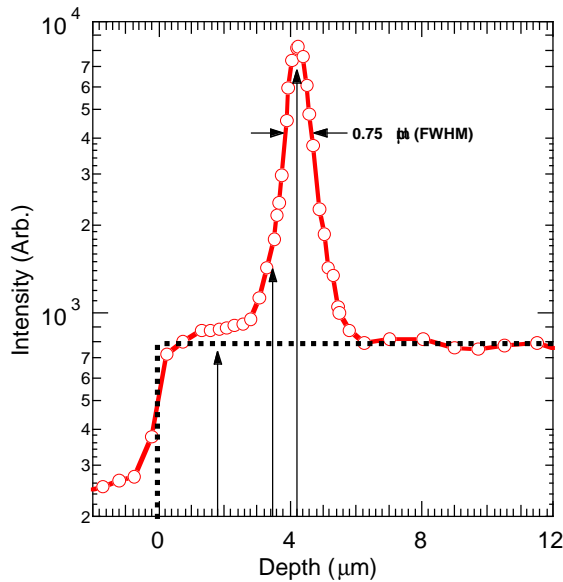


Fig. 3. Depth translation scan of the total diffuse scattering at $q = 0.04 \text{ \AA}^{-1}$ for self-ion-implanted silicon. The dashed lines indicate the sample edge and the defect free silicon scattering levels.

The arrows in Fig. 3 indicate depth positions in which detailed diffuse scattering measurements have been made as a function of $\pm q$ in $[220]$ radial directions at the (220) reflection. The net diffuse scattering (i.e. after subtracting the thermal, Compton, and Bragg tail backgrounds) for measurements at these depths has been scaled by q^4 and plotted in Fig. 4. As described above and as discussed in detail in connection with previous plan-view x-ray studies of ion implantation induced defects, the q^4 scaling emphasizes the scattering in the asymptotic region that contains the size and type sensitivity. The q^4 scaling of the $\sim q^{-2}$ Huang diffuse scattering at small- q results in a quadratic vanishing of the scattering as q goes to zero. The locally enhanced region of the nominally $\sim q^{-4}$ form of the asymptotic diffuse scattering for loops provides direct information on the size and type of the loops. The scattering intensity located at $d = 4.25$

μm below the surface strongly dominates the scattering for the range of q -values measured.

It can be inferred qualitatively from the diffuse scattering curves in Fig. 4 that the defects centered at $4.25 \mu\text{m}$ (near the range of the implanted Si) are predominantly interstitial type, since the much stronger intensity on the positive q side corresponds to lattice compression associated with interstitial loops (see Fig.1). On the other hand, the relatively weaker diffuse scattering intensities at $d = 3.45$ and $1.80 \mu\text{m}$ have more nearly equal intensities for positive and negative q , indicating the presence of an equal or larger fraction of vacancy type loops for these depths.

Analyzing the data quantitatively, the solid lines in Fig. 4 represent least-squares fits to the measured data with cross-sections calculated using Eqs. (2,3). Scattering cross-sections were calculated for vacancy and interstitial loops of radius 3.8, 11.5, 19.2, 26.9, 34.6, 42.2, and 49.9 Å, corresponding to combinations of silicon unit cells of $\{111\}$ loops. The concentrations in Eq. (3) for $R = 26.9$ and 34.6 \AA were constrained to have the same number of point defects, and similarly for $R = 42.2$, and 49.9 \AA , to limit the number of free parameters, since size resolution of a few Ångstroms is not of significance for large radii.

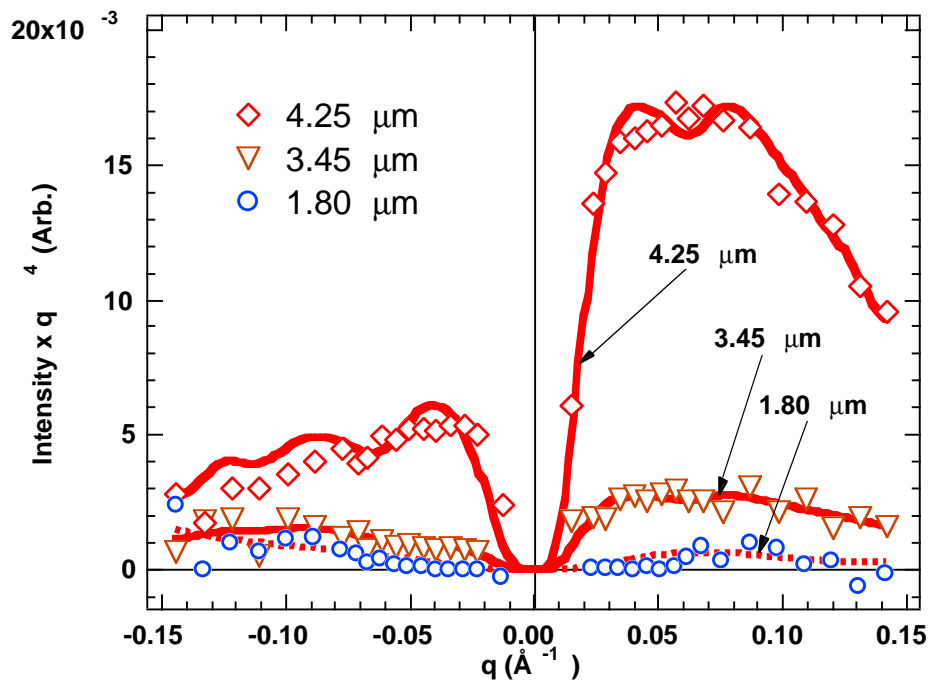


Fig. 4.. Depth resolved diffuse scattering weighted by q^4 . Measurements as a function of q were performed at three depths identified by arrows in Fig. 3. The solid lines represent least-squares fitting of the measured data to determine size distributions of vacancy and interstitial loops.

The size distributions corresponding to the solid line fits in Fig. 4 are plotted in Fig. 5. The results are presented in the form of histograms of the relative concentrations

of vacancy and interstitial loops centered at the radii of the cross-section calculations. Also included in Fig 5 are values for the relative number of point defects, N'_{PD} , contained in the loop distributions. The quantitative fits to the diffuse scattering are consistent with the qualitative interpretation of the data. That is, the number of interstitial loops in the distribution (and the number of point defects in the interstitial loops) is overwhelmingly larger than the numbers for vacancies at $d = 4.25 \mu\text{m}$. This is consistent with an expected oversupply of interstitials in this region. At $d = 1.80 \mu\text{m}$, on the other hand, the number of vacancy loops and the total number of vacancies stored in loops is larger than the corresponding numbers for interstitials. Of course, the results for the $1.80 \mu\text{m}$ position are less reliable than for the other two positions measured because of the low intensities, suggesting the need for additional measurements for a detailed analysis. Nevertheless, within the $\sim 50\%$ uncertainty in the $1.80 \mu\text{m}$ measurements, we note that the vacancy components at 3.45 and $1.80 \mu\text{m}$ are tending toward a higher ratio of vacancy to interstitials, and that the number of interstitials is lowest near the surface, both of which are consistent with expectations for this region. Considering the extremely high density in the narrow ($\sim 0.3\text{-}0.4 \mu\text{m}$) defect band observed by electron microscopy [16], it is likely that the interstitial component at $d = 3.45 \mu\text{m}$ contains a non-negligible contribution from the tail of the spatial resolution of the microbeam. The shape of the scattering profile in Fig. 2 for depths greater than the peak indicates that the $d = 1.80 \mu\text{m}$ measurement would not be significantly impacted by symmetric tails of the spatial resolution, even though the scattering intensities are quite low.

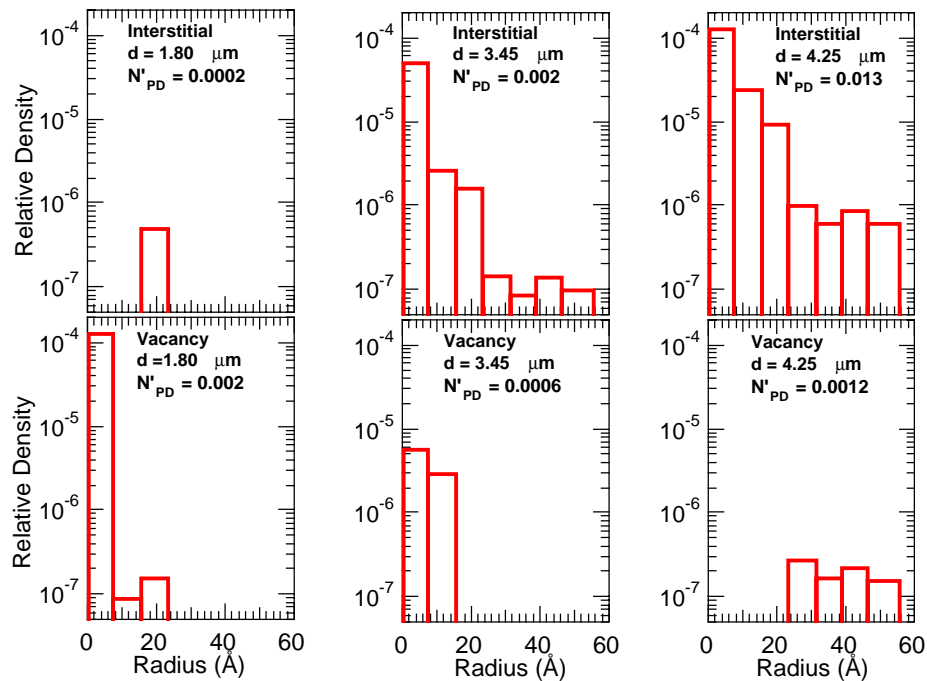


Fig. 5. Vacancy and interstitial loop size distributions corresponding to the three measurements in Fig. 4. Relative concentrations of loops and point defects contained within the loop distributions are provided.

V. Discussion

The results presented represent early stages of an ongoing investigation in which improvements in spatial resolution and measurement precision are in progress. The work performed so far demonstrates that submicron spatial resolution x-ray microbeams will be important for depth resolved studies of ion-implantation induced defects. X-ray diffuse scattering measurements such as those presented here are complementary to electron microscopy measurements in that they have sensitivity to small defect clusters that are difficult to image by electron microscopy, and for the case of dislocation loops provide a direct separation of the vacancy and interstitial components. The distinction between small vacancy and interstitial loops is exceedingly tedious by electron microscopy techniques. The x-ray technique requires some knowledge of the type of defects present in the sample in order to provide quantitative information, and information on defect types is, in general, much easier to obtain by electron microscopy than through x-ray measurements. The analysis of the diffuse scattering measurements in terms of vacancy and interstitial loops as presented here should be extended to include other defects such as small voids or vacancy aggregates as well as $\langle 311 \rangle$ interstitial platelets. Accordingly, diffuse scattering measurements will be extended to include spatially resolved small-angle scattering and Huang scattering, as well as higher precision asymptotic diffuse scattering.

Improvements in both the precision of experimental measurements and the analyses are in progress. Better spatial resolution is anticipated by the use of horizontal scattering geometry, which will make it possible to utilize the inherently smaller vertical source size of the synchrotron undulator beam. The polarization of the incident x-ray beam will preclude measurements with scattering angles close to 90° of course, and polarization corrections will be required, but spatial resolution improvements of a factor of 2 or 3 are possible.

VI. Summary

We have shown that depth resolved x-ray diffuse scattering can be used to obtain new information on the type and size distributions defect clusters in ion-irradiated silicon. The ability to obtain dislocation type information as a function of depth has been demonstrated, and size distributions for both vacancy and interstitial loops have been obtained. These measurements are complementary to electron microscopy and ion-backscattering, as well as other crystal defect investigative techniques, and combined application of such defect sensitive techniques can be expected to provide significantly increased knowledge on defect production, interaction, and thermal annealing in technologically important systems.

VII. Acknowledgements

We would like to thank W. B. Yun for Fresnel zone plate collaborations, and A. Meldrum and V. C. Venezia for TEM measurements. ORNL research was sponsored by the DOE Division of Materials Science under contract DE-AC05-96OR22464 with Lockheed Martin Energy Research Corporation. The UNICAT beamline at APS is supported by the University of Illinois, ORNL, NIST, and UOP Research & Development. The APS is supported by the DOE Office of Energy Research under contract W-31-109-ENG-38.

VIII. References

- [1] Krivoglaz, M. A. *Theory of X-Ray and Neutron Scattering by Real Crystals*, (New York, Plenum Press).
- [2] Trinkaus, H., Phys. Stat. Sol. (b), **51**, 307, (1972); Phys. Stat. Sol., **54**, 209 (1972).
- [3] Dederichs, P. H., Phys. Rev., **B1**, 1306 (1970); Dederichs, P. H. Phys. Rev., **B4**, 1041 (1971); Dederichs, P. H. J. Phys. F: Metal Phys. **3**, 471 (1973).
- [4] Trinkaus, H., Z. Angew. Phys. **31**, 229 (1971).
- [5] Ohr, S. M., J. Appl. Phys., **43**, 1361 (1972); Ohr, S. M., Phys. Stat. Sol. (b), **64**, 317 (1974)
- [6] Iida, S. and Larson, B. C., J. Mater. Res., **3**, 267 (1988).
- [7] Larson, B. C. and Schmatz, W. Phys. Stat. Sol. (b), **99**, 267 (1980).
- [8] Ehrhart, P., Trinkaus, H., and Larson, B. C., Phys. Rev. **B25**, 834 (1982).
- [9] Averbach Tony Haynes MRS volume..
- [10] Larson, B. C. and Young, F. W., Phys. Stat. Sol., (a) **104**, 273 (1987).
- [11] Krivoglaz, M. A., Phys. Met. Metallogr. **9**, 1, (1960).
- [12] Krivoglaz, M. A. and Ryaboshapka, K. P., Phys. Met. Metallogr. **16**, 643 (1963).
- [13] Barabash, R. I., and Krivoglaz, M. A., Phys. Met. Metallogr. **51**, 1, (1981).
- [14] Yoon et al. (submitted for publication)
- [15] B. Lai, B. et al, Appl. Phys. Lett. **61**, 1877 (1992);
- [16] V. C. Venezia and A. Meldrum. (unpublished).